An Epsilon-Near-Zero-Inspired PDMS Substrate Antenna With Deformation-Insensitive Operating Frequency

Zhixuan Hu, Changxing Chen, Ziheng Zhou, and Yue Li, *Senior Member, IEEE*

***Abstract*—In this letter, we transplant the epsilon-near-zero response into the design of a flexible antenna with invariant operating frequency using the magnetron sputtering and through-silicon-via crafts. The antenna is based on a section of substrate-integrated waveguide operating at its transverse TM_{100} and TM_{110} modes, to provide a difference pattern and a sum broadside pattern, respectively. The flexibility of the polydimethylsiloxane (PDMS) substrate enables the radiation pattern to be adjusted by arbitrarily bending the antenna without changing its operating frequency. The prototype operating at the TM_{100} mode around 6.58 GHz is fabricated and tested. Measured results are in agreement with the simulation, demonstrating stabilized operating frequency and radiation pattern adjustability in terms of gain, beamwidth, and mainlobe orientation. Our design may survive harsh deformation and lead to rich applications in flexible wireless electronics, such as biosensing and smart bracelet.**

***Index Terms*—Antenna radiation patterns, epsilon-near-zero (ENZ) antennas, flexible antennas, invariant operating frequency, magnetron sputtering, through-silicon-via (TSV).**

I. Introduction

WITH the capability to operate under a bent geometry, flexible antennas have generated a lot of interest in recent years [1]–[4]. Polydimethylsiloxane (PDMS), a silicon-based elastomer, has several advantages such as mechanical compliance, low dielectric constant and biocompatibility that make it a desirable candidate for bendable substrate production [5], [6]. A class of reversibly deformable antennas, with AgNWs (silver nanowires) embedded in PDMS substrates, were investigated in [7]–[9]. In [10]–[14], flexible antennas with PDMS-embedded conductive fabric substrates were proposed for wearable and transparent usages. Besides that, conformal antennas with moderate frequency stability [15]–[17] and radiation pattern adjustability [18], [19] were proposed. Previous flexible antennas are typically based on conventional printed monopoles/dipoles [3], [4], [9], [17]–[19] or thin patches [1], [2], [5]–[8], [10]–[16].

Recently, a class of media exhibiting the near-zero permittivity have drawn intensive attention for their exotic electromagnetic properties [20]–[24], which lead to novel applications [25]–[34]. Interestingly, the epsilon-near-zero (ENZ) medium supports a nearly infinite phase velocity and exhibits "static-like" field distributions independent of the operating frequency [35], [36].

In this letter, we propose a new mechanism based on the ENZ effect, to realize the flexible antenna. Different from the conventional printed flexible antennas [3], [4], [9], [17]–[19] using conductive strips to confine the currents, the ENZ medium intrinsically allows arbitrary deformation of the antenna without changing its operating frequency. A section of substrate-integrated waveguide (SIW) is employed to emulate the ENZ medium, and the antenna supports two modes, that is, the TM_{100} and TM_{110} modes, which are excited via the probe at different positions. Both modes are independent of the curvature of the antenna. Operating at the transverse cut-off TM_{100} mode, the antenna behaves effective ENZ properties [36], exhibiting a difference radiation pattern. The TM_{110} mode, on the other hand, provides a sum broadside radiation pattern. Both patterns can be adjusted with respect to the curvature by bending the flexible antenna dynamically. Furthermore, compared with the 2D-bendable ENZ antenna [37] fabricated by standard printed circuit board technique, the magnetron sputtering and through-silicon-via (TSV) crafts combined with the PDMS material are utilized to fully fulfill the potential of the geometry-irrelevant ENZ antenna. Measured results show that the antenna sustains a stabilized operating frequency even under extremely bent states close to a ring.

II. Antenna Design and Fabrication

A. Antenna Design

As illustrated in Fig. 1, the proposed antenna is realized by a section of SIW, which is composed of a 1 mm thick PDMS substrate in the middle and two metallic patches sputtered symmetrically on each side of the substrate. The PDMS used in this letter has a relative permittivity of $\varepsilon_r = 2.65$ and a loss

Manuscript received June 22, 2020; revised July 15, 2020; accepted July 19, 2020. Date of publication July 23, 2020; date of current version September 3, 2020. This work was supported in part by the National Natural Science Foundation of China under Grant 61771280, in part by the Beijing Nova Program of Science and Technology under Grant Z191100001119082, and in part by the Innovation Funds of the AFEU Department of Basic Sciences. *(Corresponding author: Yue Li.)*

Zhixuan Hu and Changxing Chen are with the Department of Basic Sciences, Air Force Engineering University, Xi'an 710051, China (e-mail: huzx012@163.com; xachenchangxing@126.com).

Ziheng Zhou and Yue Li are with the Department of Electronic Engineering, Tsinghua University, Beijing 100084, China, and also with the Beijing National Research Center for Information Science and Technology, Tsinghua University, Beijing 10084, China (e-mail: zhouzh17@mails.tsinghua.edu.cn; lyee@tsinghua.edu.cn).

Digital Object Identifier 10.1109/LAWP.2020.3011484

1536-1225 © 2020 IEEE. Personal use is permitted, but republication/redistribution requires IEEE permission.
See https://www.ieee.org/publications/rights/index.html for more information.

Authorized licensed use limited to: Yue Li. Downloaded on September 06,2020 at 06:26:01 UTC from IEEE Xplore. Restrictions apply.

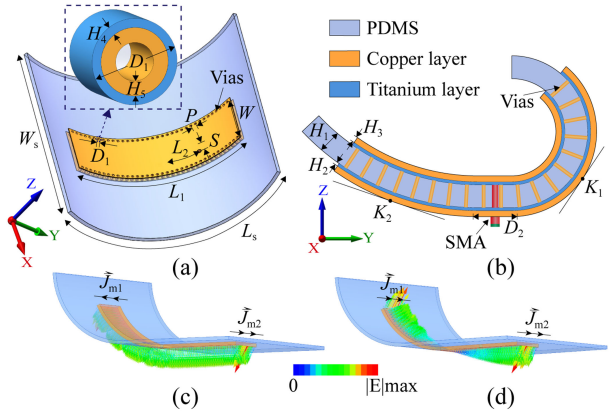

Fig. 1. (a) 3-D perspective and (b) side views of the flexible antenna under bent state. (c) Simulated 3-D E-field distributions of the antenna ($K_1 = 0, K_2 = 46.2$) operating at the cut-off TM_{100} mode around 6.58 GHz. (d) TM_{110} mode around 6.83 GHz. The effective magnetic currents are marked on the two radiating ends.

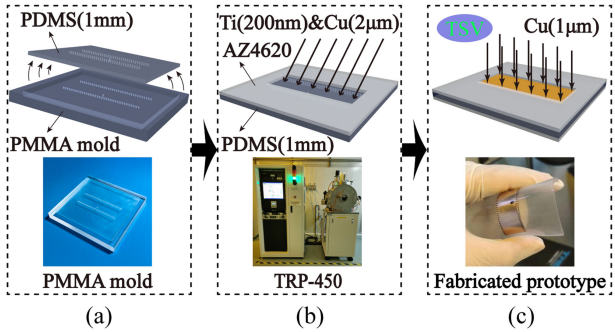

Fig. 2. Fabrication process. (a) Manufacture of PDMS substrate. (b) Printing of two copper layers on the PDMS substrate by magnetron sputtering. (c) Metallization of the internal walls of vias by TSV technique.

tangent of 0.021, measured by an Agilent 85070E Dielectric Kit in the frequency range of 6.5 to 7.0 GHz. The configuration of the antenna is shown in Fig. 1(a) and (b). As demonstrated in [36], a subwavelength narrow waveguide channel operating at the cut-off frequency of the fundamental mode exhibits the property of an ENZ medium. The dispersion property of such media, behaving zeroth-order resonance, leads to negligible dependence of its geometry.

For the TE_{10} mode of the SIW, the cut-off frequency f_0 is calculated by

$$f_0 = c/(2\sqrt{\varepsilon_r} W_{\text{eff}}) \tag{1}$$

where c is the light speed in vacuum, ε_r is the relative permittivity of the substrate and the effective width W_{eff} of the SIW is determined by [38]

$$W_{\text{eff}} = W - 1.08 \cdot D_1^2/P + 0.1 \cdot D_1^2/W \tag{2}$$

in which W is the spacing of the two arrays of metallic vias, D_1 is the diameter of the vias, and P is the periodicity of the vias. The effective relative permittivity of the SIW is given by [39]

$$\varepsilon_{\text{eff}}(f) = \varepsilon_r - c^2/(4W_{\text{eff}}^2 f^2). \tag{3}$$

Therefore, (3) can be rewritten as

$$\varepsilon_{\text{eff}}(f) = \varepsilon_r(1 - f_0^2/f^2). \tag{4}$$

In the situation when $f = f_0$, the field in the SIW will oscillate in unison and exhibit zero-phase progress, featuring the ENZ response. The parameters of the antenna are illustrated in Fig. 1(a), with the dimensions given as: $L_1 = 50$ mm, $L_s = 70$ mm, $W_s = 65$ mm, $W = 14.5$ mm, $P = 1.4$ mm, $D_1 = 0.8$ mm, $D_2 = 2$ mm, $H_1 = 1$ mm, $H_2 = 200$ nm, $H_3 = 2\ \mu$m, $H_4 = 20$ nm, and $H_5 = 1.2\ \mu$m. The antenna is fed by a 50 Ω coaxial probe, whose offset distance from the center of the patch is set as S, for tuning the impedance matching. For the TM_{100} mode operation, S and L_2 are set as 3.9 mm and 0 mm, and the operating frequency is calculated as $f_0 = 6.58$ GHz by (1). Meanwhile, under the offset of $S = 5.6$ mm and $L_2 = 12$ mm, the antenna operates at the TM_{110} mode around 6.83 GHz. The structure of the circular-arc-shape bent antenna is shown in Fig. 1(b), whose curvatures K_1 and K_2 [5] are calculated underneath the substrate on the yz plane. In the case of a circle, curvature K is inverse to the radius R ($K = 1/R$). Here, the curvature K and R represent the bending degree and curvature radius of the antenna, respectively.

B. Fabrication

The fabrication process of the antenna is shown in Fig. 2. The first step is the fabrication of the PDMS substrate. Fig. 2(a) shows the mold formed by polymethyl methacrylate. A curing agent and PDMS prepolymer (Dow Corning's Sylgard 184 silicone elastomer kit) were mixed in a 1:10 weight ratio. After that, the mixture was poured into the mold, rested for 24 h and then degassed in a vacuum desiccator for 1 h to completely remove air bubbles. Next, the solution was cured at 75°C in an oven for 3 h. After curing, the substrate was peeled off from the mold [see Fig. 2(a)]. The second step is the printing of metal films [see Fig. 2(b)]. The PDMS surface was rinsed with deionized water in advance for fear that the surface roughness might lead to uneven spin coating and metal films peeling off. Then, the photoresist AZ 4620 was used as a mask and spin-coated on the PDMS. Subsequently, the PDMS surface was modified by O_2 plasma treatment to increase oxygen groups to which the metals formed strong bonds. For later measurement purposes, the feeding hole was plugged with rubber to avoid being metalized. It was followed by two 200 nm titanium layers prior to two 2 μm copper layers sputtered on each side of the substrate. The titanium layers were sandwiched between the copper layers and PDMS to buffer stress. Inevitably, a nearly 20 nm titanium layer and a 200 nm copper-seed-layer were sputtered on each internal wall of via. The sample holder had a rotation speed of 100 r/min and the deposition rate remained almost constant, thus no fractures were observed on the conductive layer during the sputtering process. In the third step, a 1 μm copper layer was evaporated onto each seed layer with TSV technique by TRP-450 magnetron sputtering system [40] [see Fig. 2(c)]. The advanced TSV technology facilitates the metallization of the vias, which is difficult to achieve in conventional crafts. Finally, the AZ 4620 photoresist was eliminated by acetone. In the measurement, the subminiature version A (SMA) connector was inserted into the substrate and bonded to the patch with silver epoxy.

Authorized licensed use limited to: Yue Li. Downloaded on September 06,2020 at 06:26:01 UTC from IEEE Xplore. Restrictions apply.

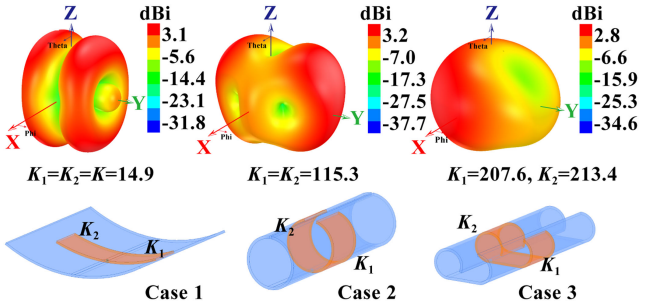

Fig. 3. Simulated 3-D realized gain patterns of the TM_{100} mode-driven antenna under symmetric bending (case 1: $K_1 = K_2$) and arbitrary bent states (cases 2 and 3) at the TM_{100} mode around $f_0 = 6.58$ GHz.

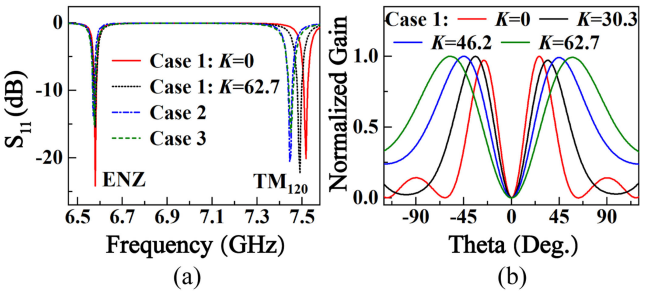

Fig. 4. (a) Simulated reflection coefficients and (b) normalized gain (in the linear scale on the *yz* plane at $f_0 = 6.58$ GHz) of the TM_{100} mode-driven antenna under different bent states.

III. Flexible Antenna Performance

A. Flexibility of Antenna at TM_{100} Mode

The 3-D electric field distribution of the antenna ($K_1 = 0$, $K_2 = 46.2$) at TM_{100} mode of 6.58 GHz is simulated by ANSYS HFSS 18.0 and shown in Fig. 1(c). It can be seen that the electric field exhibits no variation in magnitude along the SIW owing to the zeroth-order resonance in the ENZ medium. The antenna under three cases of bent states is illustrated in Fig. 3. Case 1 is symmetrical bending, with $K_1 = K_2 = K$, case 2 is an extreme state of case 1, and case 3 is arbitrary bending. The simulated reflection coefficients of the antenna with different bent states are presented in Fig. 4(a). Apparently, the frequency of TM_{100} mode exhibits no obvious shift with the change of curvature, even under cases 2 and 3. The effective magnetic currents $\vec{J}_{m1}$ and $\vec{J}_{m2}$ [marked in Fig. 1(c)] on two open ends are antiparallel at the TM_{100} mode, which leads to a difference radiation pattern (case 3 can be seen as an asymmetric difference pattern). It implies that the shape of the difference pattern can be tuned by adjusting the relative position of the two apertures with the operating frequency unmoved.

The simulated 3-D realized gain patterns of the antenna with different bent states are shown in Fig. 3. It is demonstrated in cases 1 and 2 that, as the curvature increases, the main beams of the pattern become wider, and meanwhile they are getting more distant. The simulated normalized gain of the antenna in case 1 with different curvatures on the *yz* plane is shown in Fig. 4(b). When the curvature of the antenna varies from 0 to 62.7, the angle between two main beams can be tuned from 53° to 115°.

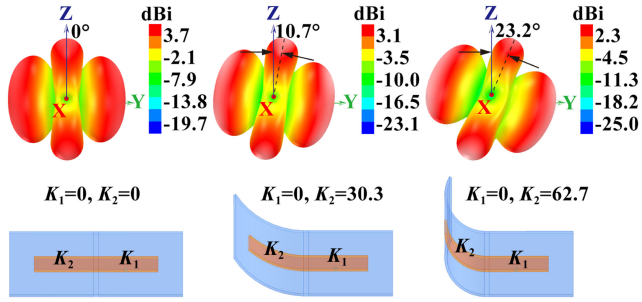

Fig. 5. Simulated 3-D realized gain patterns of the TM_{110} mode-driven antenna ($K_1 = 0$) with different K_2 at the TM_{110} mode around $f_0 = 6.83$ GHz.

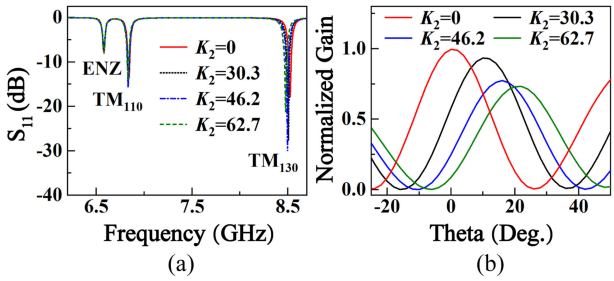

Fig. 6. (a) Simulated reflection coefficients and (b) normalized gain (in the linear scale on the *yz* plane at $f_0 = 6.83$ GHz) of the TM_{110} mode-driven antenna ($K_1 = 0$) with different curvatures K_2.

B. Flexibility of Antenna at TM_{110} Mode

The antenna operating at the TM_{110} mode exhibits the sum broadside pattern. The underlying physics is the electric fields on two radiating ends are out of phase and with equal amplitude, which contributes to a pair of parallel placed magnetic currents $\vec{J}_{m1}$ and $\vec{J}_{m2}$ with the same orientation [marked in Fig. 1(d)]. The electric field distribution of the antenna ($K_1 = 0$, $K_2 = 46.2$) at the TM_{110} mode of 6.83 GHz is shown in Fig. 1(d). With the variable K_1 staying zero and K_2 varying from 0 to 62.7, the main beam of the antenna scans from 0° to 23.2°, accompanied by the peak realized gain varying from 3.7 to 2.3 dBi, as shown in Fig. 5. A demonstration of unmoved operating frequency of TM_{110} mode with different K_2 is shown in Fig. 6(a). The simulated normalized gain of the antenna with different K_2 on the *yz* plane is illustrated in Fig. 6(b), showing the performance of beam steering by mechanically bending.

IV. Experimental Verification

Here, we validate the performance of the TM_{100} mode-driven antenna in case 1 ($K_1 = K_2 = K$) of Fig. 3. The photograph of the fabricated sample is shown in Fig. 7(a), and the antenna under arbitrary bent state is shown in Fig. 7(b). In the experiment we attach antenna to a cylinder foam with specific radius R to accurately control the curvature of the antenna, as shown in Fig. 7(c). Fig. 8 shows the measured and simulated reflection coefficients of the antenna with different curvatures. When the curvature K is lower than 96.7, the simulation and measurements are in agreement, indicating quite stable operating frequency and high quality factor of the transverse cut-off mode, with a nearly 39 MHz bandwidth for −10 dB reflection coefficient

Authorized licensed use limited to: Yue Li. Downloaded on September 06,2020 at 06:26:01 UTC from IEEE Xplore. Restrictions apply.

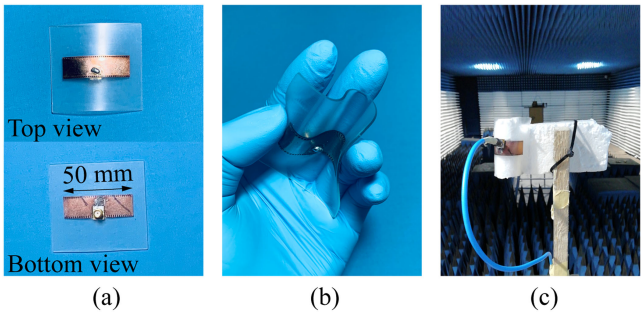

Fig. 7. (a) Photograph of the fabricated TM_{100} mode-driven antenna. (b) Fabricated prototype under arbitrary bent state. (c) Measurement setup in the anechoic chamber.

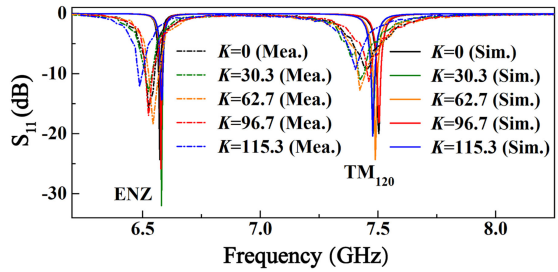

Fig. 8. Measured and simulated reflection coefficients of the antenna with different curvatures K at the TM_{100} mode.

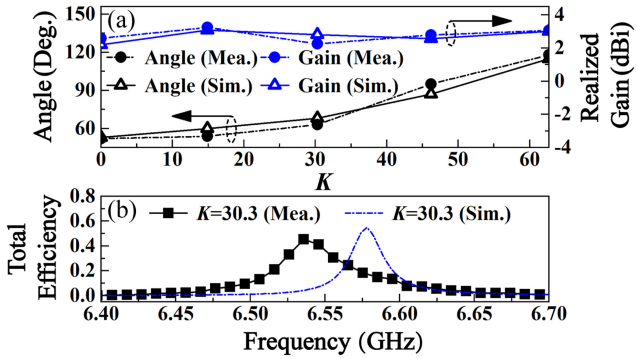

Fig. 9. (a) Measured and simulated angle between two main beams and peak realized gain versus curvature K at the TM_{100} mode. (b) Measured and simulated total efficiencies of the antenna under $K = 30.3$.

around 6.54 GHz. The wider bandwidth for -10 dB reflection coefficient in the measured results is most likely due to the increased dielectric loss of the PDMS, loss from the silver epoxy, as well as the leakage loss from the vias caused by fabrication imperfection. After testing of the antenna bent into a ring for fifty times, no conductive layer fracture was observed. The repeatability and durability qualify the proposed design for desirable flexible devices.

We have acquired measured and simulated results of the angle between two main beams and peak realized gain of the antenna as a function of curvature K, as shown in Fig. 9(a). When K varies from 0 to 62.7, the antenna exhibits a 66° (52°–118°) tuning range of the angle between two main beams, and the level of peak realized gain varies between 2.26 and 3.24 dBi. Good agreements between the simulated and measured results are

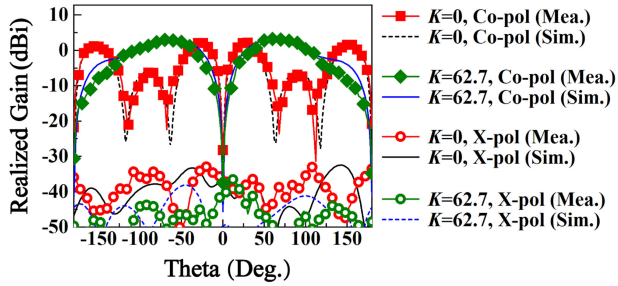

Fig. 10. Measured and simulated realized gain patterns of the antenna with different curvatures K on the yz plane operating at the TM_{100} mode.

obtained. The measured and simulated total efficiencies of the antenna ($K = 30.3$) are shown in Fig. 9(b). As seen, the prototype can reach the measured maximum efficiency about 0.45, slightly lower than the simulated result by 0.1. The loss in the result is attributed to the lossy characteristic of PDMS and fabrication errors. Conductor loss and the loss from connector also should be considered, but the dielectric loss bears responsibility for majority of losses mechanism in SIW-based structures [41]. To improve the bandwidth of the proposed antenna, thicker PDMS substrate can be used. It can be understood as the reduced quality factor accompanied by the increasing profile of the antenna. Another solution would be the reduction of permittivity of PDMS by mixing it with other material such as glass microspheres that has been successfully validated by [42].

The measured and simulated realized gain patterns of the antenna with different curvatures K on the yz plane are reported in Fig. 10. As seen, the measured radiation patterns compare well with the simulation, with the null depth about 30 dB and highest realized gain of 2.59 dBi (3.07 dBi) of the main beams at $\pm 26°$ ($\pm 59°$) under $K = 0$ ($K = 62.7$) being obtained. The angle between two beams covers a 66° tuning range when K varies from 0 to 62.7 in Fig. 10. Besides, the cross-polarization repulsions are measured higher than 32 dB on the yz plane.

V. Conclusion

In this letter, the ENZ concept is introduced into the design of a novel flexible antenna featuring invariant operating frequency and adjustable radiation pattern properties. By virtue of the advanced crafts of magnetron sputtering and TSV, the potential of the ENZ antenna is fulfilled. The two radiation characteristics, i.e., difference pattern for the center feeding and sum pattern in broadside for the offset feeding, are achieved by TM_{100} and TM_{110} modes, respectively. Measurement results show that the TM_{100} mode-driven antenna has a quite stable operating frequency of 6.54 GHz under the curvature from 0 to 96.7. The angle between two main beams of the difference pattern can be tuned from 52° to 118° with the curvature varying from 0 to 62.7. Our investigation shows that the TM_{110} mode-driven antenna offers a 0°–23.2° beam scanning range under bent scenario, with the stabilized operating frequency of 6.83 GHz. Featuring high robustness against physical deformation, the proposed antenna can be applied in various areas, such as wireless strain sensing and wearable/body-centric integrated microsystems.

Authorized licensed use limited to: Yue Li. Downloaded on September 06,2020 at 06:26:01 UTC from IEEE Xplore. Restrictions apply.

REFERENCES

[1] A. S. M. Alqadami, N. Nguyen-Trong, B. Mohammed, A. E. Stancombe, M. T. Heitzmann, and A. Abbosh, "Compact unidirectional conformal antenna based on flexible high-permittivity custom-made substrate for wearable wideband electromagnetic head imaging system," *IEEE Trans. Antennas Propag.*, vol. 68, no. 1, pp. 183–194, Jan. 2020, doi: 10.1109/TAP.2019.2938849.

[2] G. J. Hayes, S. Ju-Hee, A. Qusba, M. D. Dickey, and G. Lazzi, "Flexible liquid metal alloy (EGaIn) microstrip patch antenna," *IEEE Trans. Antennas Propag.*, vol. 60, no. 5, pp. 2151–2156, May 2012, doi: 10.1109/TAP.2012.2189698.

[3] C. Shi, W. Zhigang, P. Hallbjorner, K. Hjort, and A. Rydberg, "Foldable and stretchable liquid metal planar inverted cone antenna," *IEEE Trans. Antennas Propag.*, vol. 57, no. 12, pp. 3765–3771, Dec. 2009, doi: 10.1109/TAP.2009.2024560.

[4] R. B. V. B. Simorangkir, D. Le, T. Bjorninen, A. S. M. Sayem, M. Zhadobov, and R. Sauleau, "Washing durability of PDMS-conductive fabric composite: Realizing washable UHF RFID tags," *IEEE Antennas Wireless Propag. Lett.*, vol. 18, no. 12, pp. 2572–2576, Dec. 2019, doi: 10.1109/LAWP.2019.2943535.

[5] L. Chih-Peng, C. Chieh-Hsiang, Y. T. Cheng, and C. F. Jou, "Development of a flexible SU-8/PDMS-based antenna," *IEEE Antennas Wireless Propag. Lett.*, vol. 10, pp. 1108–1111, 2011, doi: 10.1109/LAWP.2011.2170398.

[6] A. S. M. Alqadami, M. F. Jamlos, P. J. Soh, and G. A. E. Vandenbosch, "Assessment of PDMS technology in a MIMO antenna array," *IEEE Antennas Wireless Propag. Lett.*, vol. 15, pp. 1939–1942, 2016, doi: 10.1109/LAWP.2015.2513960.

[7] L. Song, A. C. Myers, J. J. Adams, and Y. Zhu, "Stretchable and reversibly deformable radio frequency antennas based on silver nanowires," *ACS Appl. Mater. Interfaces*, vol. 6, no. 6, pp. 4248–53, Mar. 2014.

[8] T. Rai, P. Dantes, B. Bahreyni, and W. S. Kim, "A stretchable RF antenna with silver nanowires," *IEEE Electron. Device Lett.*, vol. 34, no. 4, pp. 544–546, Apr. 2013.

[9] Z. H. Jiang, Z. Cui, T. Yue, Y. Zhu, and D. H. Werner, "Compact, highly efficient, and fully flexible circularly polarized antenna enabled by silver nanowires for wireless body-area networks," *IEEE Trans. Biomed. Circuits Syst.*, vol. 11, no. 4, pp. 920–932, Aug. 2017, doi: 10.1109/TBCAS.2017.2671841.

[10] R. B. V. B. Simorangkir, A. Kiourti, and K. P. Esselle, "UWB wearable antenna with a full ground plane based on PDMS-Embedded conductive fabric," *IEEE Antennas Wireless Propag. Lett.*, vol. 17, no. 3, pp. 493–496, Mar. 2018, doi: 10.1109/LAWP.2018.2797251.

[11] R. B. V. B. Simorangkir, Y. Yang, K. P. Esselle, and B. A. Zeb, "A method to realize robust flexible electronically tunable antennas using polymer-embedded conductive fabric," *IEEE Trans. Antennas Propag.*, vol. 66, no. 1, pp. 50–58, Jan. 2018, doi: 10.1109/TAP.2017.2772036.

[12] H. A. Elmobarak Elobaid, S. K. Abdul Rahim, M. Himdi, X. Castel, and M. Abedian Kasgari, "A transparent and flexible polymer-fabric tissue UWB antenna for future wireless networks," *IEEE Antennas Wireless Propag. Lett.*, vol. 16, pp. 1333–1336, 2017, doi: 10.1109/LAWP.2016.2633790.

[13] A. S. M. Sayem, R. B. V. B. Simorangkir, K. P. Esselle, and R. M. Hashmi, "Development of robust transparent conformal antennas based on conductive mesh-polymer composite for unobtrusive wearable applications," *IEEE Trans. Antennas Propag.*, vol. 67, no. 12, pp. 7216–7224, Dec. 2019, doi: 10.1109/TAP.2019.2930116.

[14] R. B. V. B. Simorangkir, Y. Yang, L. Matekovits, and K. Esselle, "Dual-band dual-mode textile antenna on pdms substrate for body-centric communications," *IEEE Antennas Wireless Propag. Lett.*, vol. 16, pp. 677–680, 2017, doi: 10.1109/LAWP.2016.2598729.

[15] A. Arif, M. Zubair, M. Ali, M. U. Khan, and M. Q. Mehmood, "A compact, low-profile fractal antenna for wearable on-body WBAN applications," *IEEE Antennas Wireless Propag. Lett.*, vol. 18, no. 5, pp. 981–985, May 2019, doi: 10.1109/LAWP.2019.2906829.

[16] R. Quarfoth, Y. Zhou, and D. Sievenpiper, "Flexible patch antennas using patterned metal sheets on silicone," *IEEE Antennas Wireless Propag. Lett.*, vol. 14, pp. 1354–1357, 2015, doi: 10.1109/LAWP.2015.2406887.

[17] S. Ahmed, F. A. Tahir, A. Shamim, and H. M. Cheema, "A compact kapton-based inkjet-printed multiband antenna for flexible wireless devices," *IEEE Antennas Wireless Propag. Lett.*, vol. 14, pp. 1802–1805, 2015, doi: 10.1109/LAWP.2015.2424681.

[18] H. P. Phan, T. P. Vuong, P. Benech, P. Xavier, and P. Borel, "Study of bending effects of a wideband paper-based printed microstrip-fed antenna," *Microw. Opt. Technol. Lett.*, vol. 62, no. 4, pp. 1785–1794, 2020.

[19] L. Marnat and A. Shamim, "Liquid Crystal Polymer (LCP) based antenna for flexible system on package (SoP) applications," in *Proc. 15th Int. Symp. Antenna Technol. Appl. Electromagn.*, Jun. 25–28, 2012, pp. 1–4.

[20] S. Enoch, G. Tayeb, P. Sabouroux, N. Guerin, and P. Vincent, "A metamaterial for directive emission," *Phys. Rev. Lett.*, vol. 89, no. 21, Nov. 2002, Art. no. 213902.

[21] R. W. Ziolkowski, "Propagation in and scattering from a matched metamaterial having a zero index of refraction," *Phys. Rev. E*, vol. 70, no. 4, 2004, Art. no. 046608.

[22] I. Liberal, A. M. Mahmoud, Y. Li, B. Edwards, and N. Engheta, "Photonic doping of epsilon-near-zero media," *Science*, vol. 355, no. 6329, pp. 1058–1062, Mar. 2017.

[23] Y. Li, I. Liberal, C. Della Giovampaola, and N. Engheta, "Waveguide metatronics: Lumped circuitry based on structural dispersion," *Sci. Adv.*, vol. 2, no. 6, 2016, Art. no. e1501790.

[24] Y. Li and N. Engheta, "Supercoupling of surface waves with ε-near-zero metastructures," *Phys. Rev. B*, vol. 90, no. 20, 2014, Art. no. 201107.

[25] D. Li, Z. Szabo, X. Qing, E.-P. Li, and Z. N. Chen, "A high gain antenna with an optimized metamaterial inspired superstrate," *IEEE Trans. Antennas Propag.*, vol. 60, no. 12, pp. 6018–6023, Dec. 2012, doi: 10.1109/TAP.2012.2213231.

[26] D. Mitra, A. Sarkhel, O. Kundu, and S. R. B. Chaudhuri, "Design of compact and high directive slot antennas using grounded metamaterial slab," *IEEE Antennas Wireless Propag. Lett.*, vol. 14, pp. 811–814, 2015.

[27] X. Zhang and Z. Liu, "Superlenses to overcome the diffraction limit," *Nature Mater.*, vol. 7, no. 6, pp. 435–441, Jun. 2008.

[28] J. C. Soric and A. Alu, "Longitudinally independent matching and arbitrary wave patterning using ε-near-zero channels," *IEEE Trans. Microw. Theory Techn.*, vol. 63, no. 11, pp. 3558–3567, Nov. 2015.

[29] F. Benz *et al.*, "Single-molecule optomechanics in 'picocavities'," *Science*, vol. 354, no. 6313, pp. 726–729, Nov. 2016.

[30] A. K. Jha and M. J. Akhtar, "Design of multilayered epsilon-near-zero microwave planar sensor for testing of dispersive materials," *IEEE Trans. Microw. Theory Techn.*, vol. 63, no. 8, pp. 2418–2426, Aug. 2015.

[31] A. Dadgarpour, M. S. Sorkherizi, T. A. Denidni, and A. A. Kishk, "Passive beam switching and dual-beam radiation slot antenna loaded with ENZ medium and excited through ridge Gap waveguide at millimeter-waves," *IEEE Trans. Antennas Propag.*, vol. 65, no. 1, pp. 92–102, Jan. 2017, doi: 10.1109/TAP.2016.2631140.

[32] D. M. George, A. Chandroth, C. C. H. Ng, and P. R. Young, "High-gain narrow-band slotted antenna based on ENZ SIW structure," *J. Phys. D, Appl. Phys.*, vol. 51, no. 13, 2018.

[33] Z. Zhou, Y. Li, H. Li, W. Sun, I. Liberal, and N. Engheta, "Substrate-integrated photonic doping for near-zero-index devices," *Nature Commun.*, vol. 10, no. 1, Sep. 2019, Art. no. 4132.

[34] M. Silveirinha and N. Engheta, "Tunneling of electromagnetic energy through subwavelength channels and bends using ε-near-zero materials," *Phys. Rev. Lett.*, vol. 97, no. 15, Oct. 2006, Art. no. 157403.

[35] N. Engheta, "Pursuing near-zero response," *Science*, vol. 340, no. 6130, pp. 286–7, Apr. 2013.

[36] B. Edwards, A. Alu, M. E. Young, M. Silveirinha, and N. Engheta, "Experimental verification of epsilon-near-zero metamaterial coupling and energy squeezing using a microwave waveguide," *Phys. Rev. Lett.*, vol. 100, no. 3, Jan. 2008, Art. no. 033903.

[37] Z. Zhou and Y. Li, "Effective epsilon-near-zero (ENZ) antenna based on transverse cutoff mode," *IEEE Trans. Antennas Propag.*, vol. 67, no. 4, pp. 2289–2297, Apr. 2019, doi: 10.1109/TAP.2019.2894335.

[38] X. Feng and W. Ke, "Guided-wave and leakage characteristics of substrate integrated waveguide," *IEEE Trans. Microw. Theory Techn.*, vol. 53, no. 1, pp. 66–73, Jan. 2005, doi: 10.1109/TMTT.2004.839303.

[39] W. Rotman, "Plasma simulation by artificial dielectrics and parallel-plate media," *IRE Trans. Antennas Propag.*, vol. AP-10, no. 1, pp. 82–95, 1962.

[40] Sky Technology Development, "TRP-450 magnetron sputtering system." 2020. [Online]. Available: http://www.sky.ac.cn/index.php?ac=article&at=read&did=279

[41] D. Zheng, Y.-L. Lyu, and K. Wu, "Longitudinally slotted SIW leaky-wave antenna for low cross-polarization millimeter-wave applications," *IEEE Trans. Antennas Propag.*, vol. 68, no. 2, pp. 656–664, Feb. 2020, doi: 10.1109/TAP.2019.2940469.

[42] W. A. W. Muhamad, R. Ngah, M. F. Jamlos, P. J. Soh, and M. T. Ali, "High-gain dipole antenna using polydimethylsiloxane–glass microsphere (PDMS-GM) substrate for 5G applications," *Appl. Phys. A*, vol. 123, no. 1, 2016.

Authorized licensed use limited to: Yue Li. Downloaded on September 06,2020 at 06:26:01 UTC from IEEE Xplore. Restrictions apply.